Chapter 13

Organic Nanotubes: Promising Vehicles for Drug Delivery

Utpal Bhadra, Manika Pal Bhadra,
Jagannadh Bulusu and J.S. Yadav

Additional information is available at the end of the chapter

http://dx.doi.org/10.5772/58412

1. Introduction

1.1. Nano particles and drug delivery

Nanostructured materials, due to the 'size effect' [1] and flexible surface modifications, demonstrate unique properties. The surface chemistry and quantum effects of nanomaterials give rise to novel electronic, optical and magnetic properties and thus have become attractive for their applications *in vivo* imaging and diagnostics, regenerative medicine, infection biology, neuroelectronics and biosensors [2, 3]. Functional organic molecules self-assemble into well-defined nanostructures have become a fast developing field due to its similarity with the natural biological processes but also to produce a new range of materials with many application possibilities. Studies have shown that the self-assembling molecular scaffolds like peptides, lipids and other organic scaffolds, on the basis of different non-covalent interactions (π-π interaction, van der Waals, hydrogen bonding, hydrophilic/hydrophobic and electrostatic) can spontaneously associate to form nanomaterials with various morphologies, like nanotubes, nanospheres, nanofibrils, nanorods, nanotapes, and nanovesicles under different conditions [4, 5, 6]. These nanomaterials made from simple building blocks, can be tuned to present interesting physicochemical properties owing to their biocompatibility, capability of specific molecular recognition, easy availability, and functional flexibility. They offer several advantages as mass delivery agents due to their size, which allows them to cross biological barriers and their chemical versatility makes them suitable for loading a wide range of substances enabling multifunctionality [7].

Several biomaterials have been studied that show a greater promise in nanomedicine including quantum dots [8, 9], carbon nanotubes, coupling of quantum dots and carbon nanotubes [10]

gold nanoparticles [11], silica nanoparticles [12], organic polymers [13], bi-or multilayer liposomes (14), magnetic and magnetofluorescent nanoparticles [15], silica nanoparticles [16]. These studies have highlighted the importance of the role of nanomaterial size, shape, material composition, surface chemistry; the choice of the cell type for the study; the effect of nanomaterial-cell interactions, the fate of the nanomedicines and the resulting cellular responses [17, 18]. But each material has its own limitation in biological systems. The complexity of interaction between nanomaterials and cellular environment, biocompatibility, their progressive accumulation in live cells, inefficient bio-degradation and other pharmacokinetic properties including cell toxicity and immunogenicity presents a variety of obstacles for choosing the specific nanomaterials for testing. Considerable efforts have been directed towards surface modifications [19], multivalent attachment of small molecules [20] and coating for minimizing such effects. These measures also favour *in vivo* distribution through diversified biological organs and effective tissue specific targeting. Though use of nano-materials have been successful in *in vitro* cultured cells, its *in vivo* application by repeated injections is more challenging for shelf life, potential immunogenecity, biocompatibility and other physiological hurdles. An alternate approach for tracking the micro device through complex organs is via oral ingestion followed by better absorption and systemic spreading through body fluid instead of repeated intravenous injections.

2. Advantages of nanotubes

Nanotubes, hollow cylindrical nanostructures are promising drug carriers offering many advantages over other drug delivery systems. Nanotubes, which have separated inner and outer surfaces, can be differentially functionalized either to load desired molecules inside or by suitably designing the chemical features of the outer surface allows for site-specific drug delivery. Relevant attachments include biologically active molecules, targeting sequences, intrinsic fluorescent or other imaging devices, biocompatible coatings, and others. Major focus in the development of nanotubes for biomaterial delivery relies on three important factors, chemical modification, biocompatibility and minimal damage of the harbouring environment. To date, the potential use of drug components for synthesizing the microstructure has not been realized primarily because of lack of methods for self-assembly to form a tubular structure and coupling them with tracking fluorescence markers.

3. PABA nanotubes

The core or the building block is an important component in biomaterial development. p-aminobenzoic acid (PABA) is frequently found as a structure moiety in drugs (in a database of 12111 commercial drugs, 1.5% (184 drugs) were found to contain the PABA moiety that have a wide range of therapeutic uses [21]. To minimize the problem of biocompatibility and cell toxicity, a more reliable choice is to select building blocks that can be used for developing a library of nanomaterials, which will have functional and structural diversity. We have chosen

http://dx.doi.org/10.5772/58412

PABA as the molecular building block with appropriate chemical saturated or unsaturated fatty acid substitution to build a library of PABA based nanomaterials for potential use as drug delivery systems.

We have synthesized 4-N-pyridin-2-yl-benzamides from p-nitrobenzoic acid [22]. The synthesis involved amide formation with 2-aminopyridine followed by reduction of the nitro functionality utilizing a standard protocol using Pd/C under hydrogen atmosphere as the reducing agent. Subsequently, the free amine functionality present in benzamide was coupled with seven different acid chlorides (undecanoyl chloride, C=11; undec-10-enoyl chloride, C=11;1, Lauroyl chloride, C=12, Miristoyl Chloride, C=14, Palmetoyl chloride, C=16, Stearoyl chloride, C=18 and Oleoyl chloride C=18:1) to furnish the corresponding 4-alkylamido-N-pyridin-2-yl benzamides respectively hereafter referred to as C11, C11U, C12, C14, C16, C18 and C18U based on the length of the side chains and unsaturated moieties coupled during synthesis. Synthesis of the Lauroyl chlrode and stearoyl chloride is shown in Figure 1.

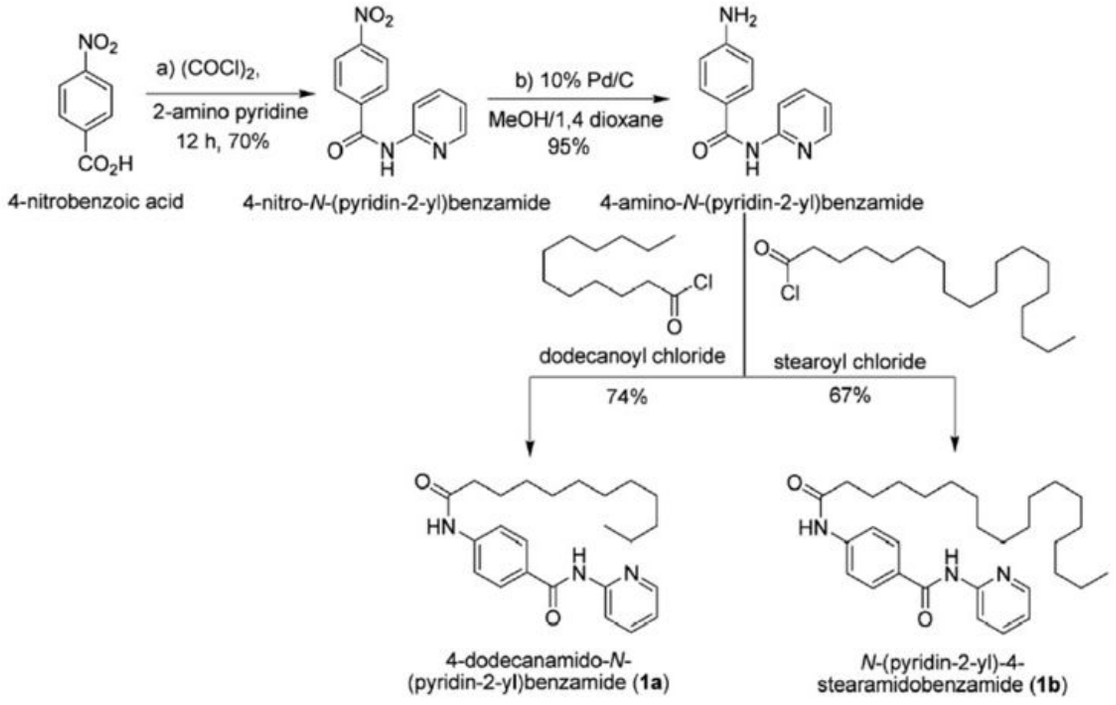

Figure 1. Synthesis of Lauroyl chlrode and stearoyl chloride

The seven alkyl benzamides (1 mg) were added to methanol (2 ml) and heated to 60 ◦C till it dissolved completely. Deionized water (2 ml) was added slowly at the same temperature to obtain a milky white solution which, upon gradually cooling to room temperature, furnished cotton-like white aggregates. Three of the nanoaggregates exhibited intrinsic fluorescence (C11, C6 and C18) and to prepare rhodamine-B embedded Benzamide nanotubes (C11U, C12,C14, C18U) compounds, rhodamine B solution (0.1 ml, 1 mg of rhodamine B in 5.0 ml of deionized water) was added prior to the addition of deionized water (2 ml) which, on cooling,

produced pink-coloured aggregates. The aggregates were isolated under centrifuged conditions (4500 rpm for 20 min) followed by overnight drying at 60 ◦C to afford 0.5 mg of the final nanomaterials. All the PABA based nanomaterials C11, C11U, C12, C14. C16, c18 and C18U studied obtained by side chain variation are shown in Figure 2.

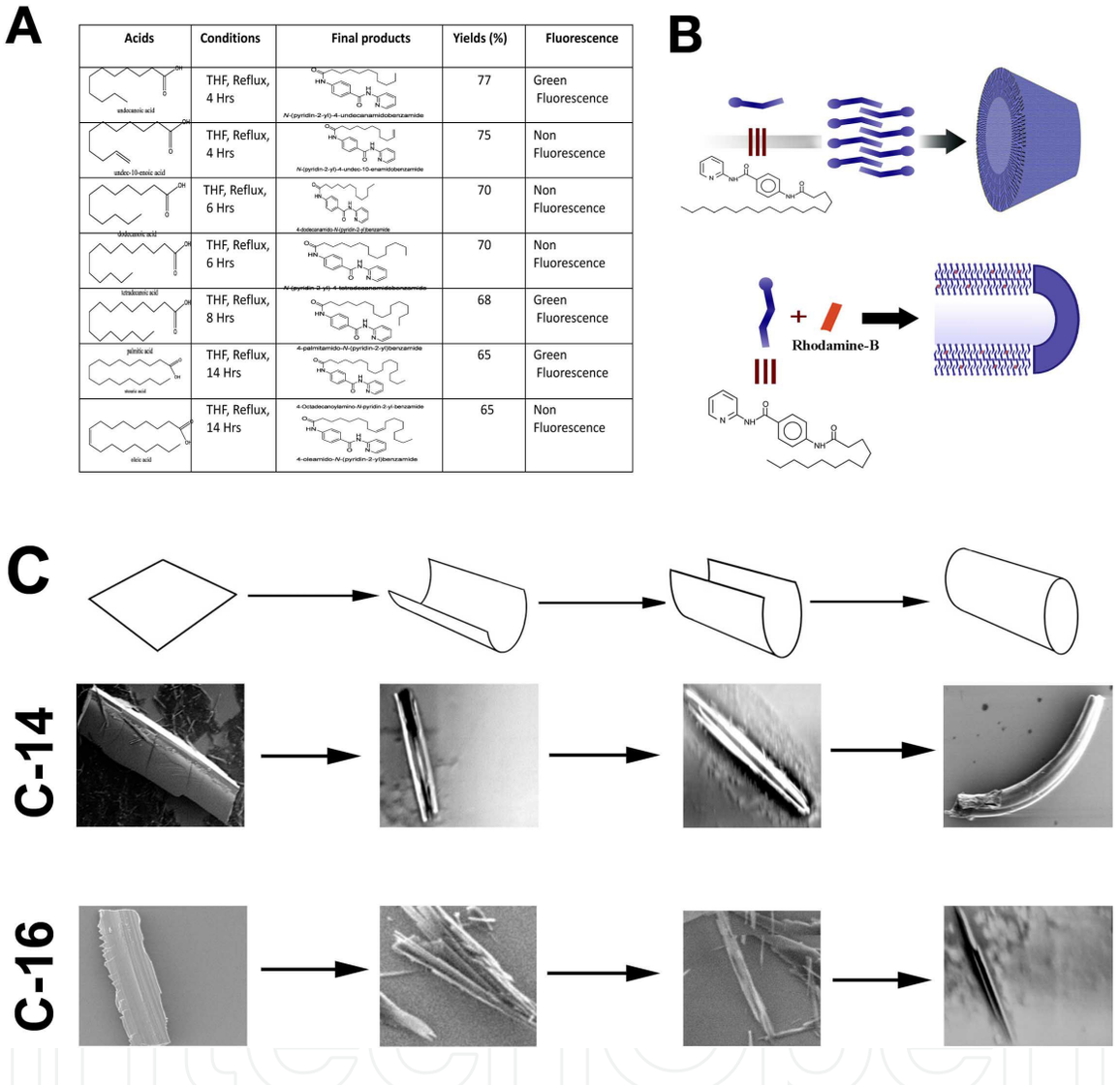

Acids	Conditions	Final products	Yields (%)	Fluorescence
undecanoic acid	THF, Reflux, 4 Hrs	N-(pyridin-2-yl)-4-undecanamidobenzamide	77	Green Fluorescence
undec-10-enoic acid	THF, Reflux, 4 Hrs	N-(pyridin-2-yl)-4-undec-10-enamidobenzamide	75	Non Fluorescence
dodecanoic acid	THF, Reflux, 6 Hrs	4-dodecanamido-N-(pyridin-2-yl)benzamide	70	Non Fluorescence
tetradecanoic acid	THF, Reflux, 6 Hrs	N-(pyridin-2-yl)-4-tetradecanamidobenzamide	70	Non Fluorescence
palmitic acid	THF, Reflux, 8 Hrs	4-palmitamido-N-(pyridin-2-yl)benzamide	68	Green Fluorescence
stearic acid	THF, Reflux, 14 Hrs	4-Octadecanoylamino-N-pyridin-2-yl-benzamide	65	Green Fluorescence
oleic acid	THF, Reflux, 14 Hrs	4-oleamido-N-(pyridin-2-yl)benzamide	65	Non Fluorescence

Figure 2. Design and chemical synthesis of nanomaterials. (A) chemical structure of acid side chains, final self assembled product reaction condition, percentage of yield, fluorescent dyes summarized in a table. (B) Schematic diagram showing formation of two nanoparticles (C12 and C18) was drawn (C) Routine diagram and compatible SEM images showing rollover mechanism of two nanomaterial (C-14 and C16) formation.

Prior to the study of the cellular uptake of the seven nanomaterials which use the PABA template, a study was also undertaken to observe whether the biological properties of PABA changed due to the side chain substitution and self-assembly. The biological properties of PABA in self-assembled conjugates as monitored by the growth and viability of the wild type bacterial strains (E. coli K12) in cultured media in the presence of PABA or PABA containing nanostructures. A similar level of bacterial growth in culture media containing PABA or PABA

nanomaterials revealed that modifications and subsequent formation of PABA based biomaterials did not result in change of properties.

Scanning electron microscopy (SEM), transmission electronic microscopy (TEM) and atomic force microscopy (AFM) and dynamic light scattering (DLS) were used to investigate the structural and morphological properties of the self-assembled nanomaterials. The TEM and SEM characterization suggest that the nanomaterials self-assembled using saturated acid side chains mainly form tubular structures with a hollow space inside, while those self-assembled from unsaturated side chains produced cube shaped particles (Figure 3). The mechanism of nanotubes formed by acid chlorides with saturated side chains is believed to that initially, they aggregate into sheets which later transform to curved structures and join to form nanotubes. This nanotube formation mechanism was also confirmed from a low-angle powder X-ray diffraction studies carried out on the of self-assembly of para-terphenylen-1,4''-ylenebis (dodecanamide) and the results have shown that self-assembly results in layered sheets or rolled up nanotubes dependent on the experimental conditions [23]. Recently a frustrated aggregate internal rearrangement (FAIR) mechanism was also proposed for organic nanotube formation [24]. The authors suggested from density functional calculations that self-assembly takes place by forming sheet like structures driven by nonspecific and nondirectional intermolecular interactions with weak intermolecular H-bonds providing additional stability to the structure. Instead of the fully formed H-bonded structure, the partially formed hydrogen bonded layers to avoid kinetic energy traps transform to curved structures. Mechanism by which the self-assembly of C11U and C18U results in the formation of cubic structures is also not known. It can be surmised however that like the tubular structure formation, the cubic structures also form by unidirectional growth of the sheets by the chemical subunits, followed by the folding of sheets into cubes by penalties that are compensated by favoured binding energies [25].

To ascertain the size, a Dynamic Light-Scattering (DLS) study was carried out using different nanoparticles produced by side chain variation. In all cases, freshly prepared nanomaterials were mostly uniform in size with very few submicron sized aggregates, while materials examined after prolonged storage (after 3 days) contains more micron sized aggregates. DLS studies from fresh preparations estimated an average size in the range of 100 to 200 nm but prolonged storage leads to the formation of submicron-sized structures. The average height of each nanoparticle as measured by 3 D reconstituted AFM images is 3-5 nm.

4. Characterisation of nanoparticles

Laser confocal microscopic images showed that three nanostructures, C-11, C-16 and C-18 emitted intrinsic green fluorescence, while remaining four nanomaterials (C-11U, C-12, C-14, C-18U) do not emit any intrinsic fluorescence (Figure 3). To verify the fluorescence enhancement, induced by self-assembly nanostructure, the fluorescence emission of the monomer and the self-assembled nanoparticles were compared using Nanodrop 3300 fluoro-spectrometer. The fluorescence intensity of the nanostructures (determined by a methanol/water solution)

using blue diode option (maximum excitation 477 nm) was much stronger and found in 510 nm than that of the non-fluorescent monomer (studied in CH2Cl2, where it does not aggregate) under the same 0.3 wt % concentration.

5. Relative uptake of nanomaterials in insect and human cell lines

We have carried out a systematic and comparative study on the relative uptake and estimation of the accumulated nanomaterials of varying composition and size inside the subcellular organelles by fluorescence microscopy, confocal laser scanning microscopy, and fluorometry. Three model cell lines representing different physiological function (insect and human) were chosen for the investigation. Drosophila S2 was chosen as a model as they are phagocytic cells and have a high cotransfection rate and for the mammalian cell lines HeLa cancer cells and the nonneoplastic Human Embryonic Kidney (HEK-293) were chosen for the study. The cell lines were cultured in media containing different concentrations of the nanomaterial; 10 μg/ml, 30 μg/ml and 60 μg/ml in 0.01% DMSO. In all cases, nanomaterial containing media to a final concentration 60 μg/ml in 0.01% DMSO showed no adverse effect on cell physiology.

In general, basic cell physiology and cell surveillance do not allow easy accessibility of foreign particles inside the cells. Exhaustive efforts are being carried out for engineering smooth delivery vehicles, synthesized from biocompatible and biodegradable materials. Though use of nano-materials has been successful in in vitro cultured cells [26], in practice, its adaptability in in vivo organ tracking by repeated injections is more challenging because of its limited self-life, delivery hurdles, and compatibility to fragile cell environment and potent immunogenicity [19]. Major improvements on chemical modifications of nano-materials play a fundamental role in cell uptake and live tissue distribution [27]. The surface texture by using small molecules, side chains and other conjugates alter the biological properties of nanoparticles [20]. We therefore hypothesized that such variation could increase smooth transition to shuttle inside live cells. To date, efforts for surface modifications of organic nanostructures have been rare. It is mainly due to lack of self-assembled organic molecules and compatibility of small molecules with nanoskeleton [29. 30].

Accumulation of nanomaterials varied widely based on the side chains of PABA conjugates inside both insect (Drosophila S2) and human (HEK293, HeLa) cells. It was observed that nanoparticles, which emit intrinsic green fluorescence (C-11, C-16 and C-18) accumulate almost equally in all three cell types despite the differences in the length of carbon side chains (Figure 4). These results suggest that the tubular shape of all three nanostructures is more important than the length of the acid chains for cell entry. The accumulation increased proportionately to the concentration of incubated nanoparticles and time. Moreover, uptake of nanotubes C-12 and C-14, are more intense relative to unsaturated acid chains (C-11U and C-18U) in human cells. It is possible that PANA nanomaterials with unsaturated side chain might hinder the cellular entry. In contrast, a distinct internal cell environment of Drosophila S2 cells increases the uptake of unsaturated C-11U particles. These results demonstrated that three major factors; shape, properties associated with unsaturated side chain and cross species cell physiology are involved in the rate of cellular uptake.

http://dx.doi.org/10.5772/58412

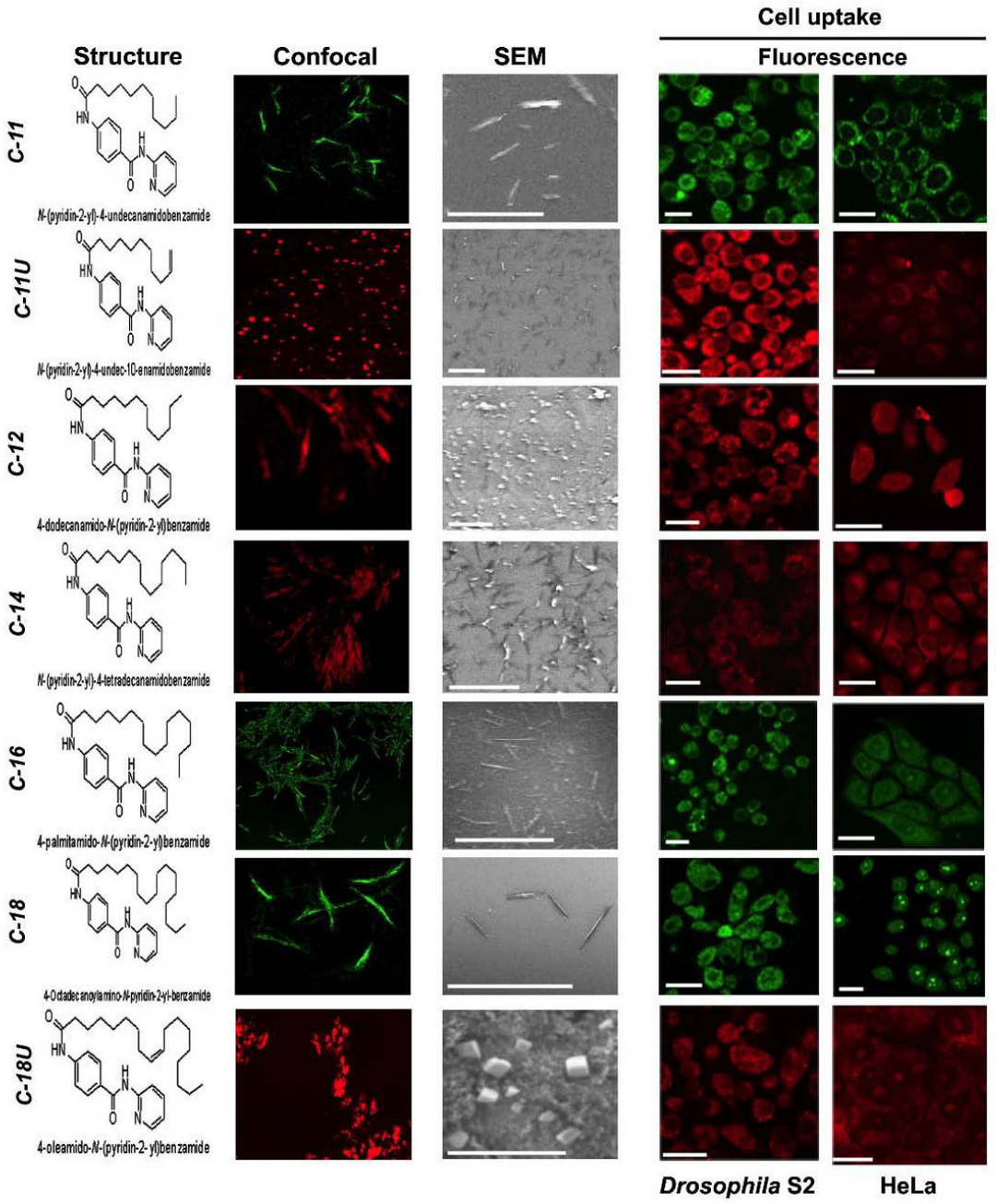

Figure 3. Physico-chemical properties and microscopic views of seven PABA anomaterials. elative Uptake of several nanomaterials in insect (Drosophila S2) and human tumour cells (HeLa) were shown. The differences in chemical structure, shape and surface texture of nanomaterials leads to a variation in cell uptake. Scale-250 nm (SEM), 50 µm (cells)

Since rhodamine was not covalently bonded with nanostructures C11U, C12, C14 and C18U, we cannot rule out the possibility that they might leach the dye from the nanostructures during cell uptake. Total fluorescence intensity in cells following exposure to the nanoparticle solutions could be due to the presence of nanoparticles through the cell, rather than correctly assigned to either a combination of free-dye and nanoparticle-bound dye, or even entirely to free dye, we incubated both the insect and human cells with rhodamine dye as well as

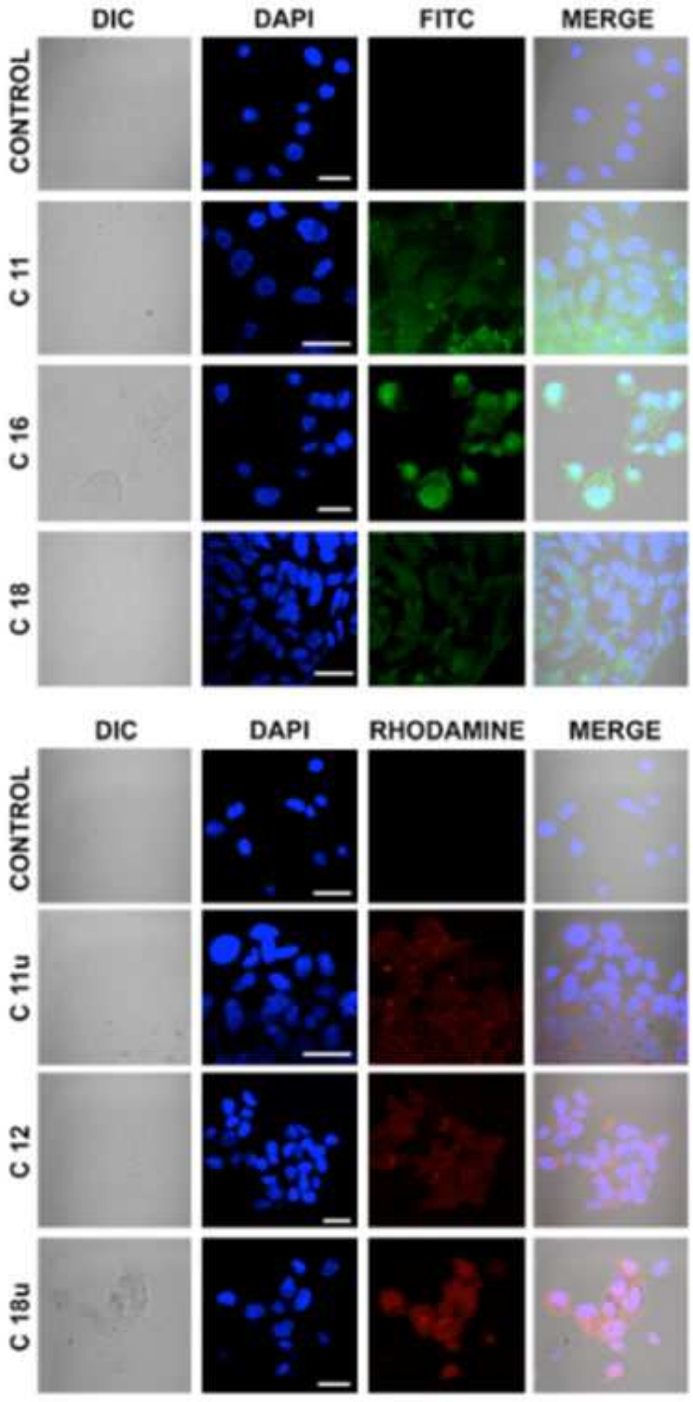

Figure 4. Biocompatibility of nanoparticles in nonneoplastic (HEK-293) Human Embryonic Kidney cells. Specificity of cellular uptake of different nanoparticles in HEK-293 cells was shown. The cells were incubated in 0.1% DMSO (control) and 60mg/ml of each nanoparticle containing culture media separately for 12 hrs prior to process. The cells were counterstained with DAPI. The DIC images and merge figures were shown in the left and right sides of the panel. Scale 40µm

rhodamine bound nanomaterials (C-11U and C-14) separately under same experimental conditions. After equal period of incubation, cells from both conditions were processed and viewed under confocal microscope. Cells cultured with only rhodamine showed accumulation at the outer periphery with negligible amount inside, while an intense fluorescence was seen inside the cells cultured with rhodamine containing nanoparticles indicating that rhodamine dye did not leached and was entrapped or contained in the nanotubes and nanocubes. (can we make this statement If all of the dye is nanoparticle bound then the nanoparticles are localized in sub-cellular oraganelles and where as if these system contains a significant amounts of free dye then fluorescence is distributed throughout the cell across cell barriers and into the cytoplasm.)

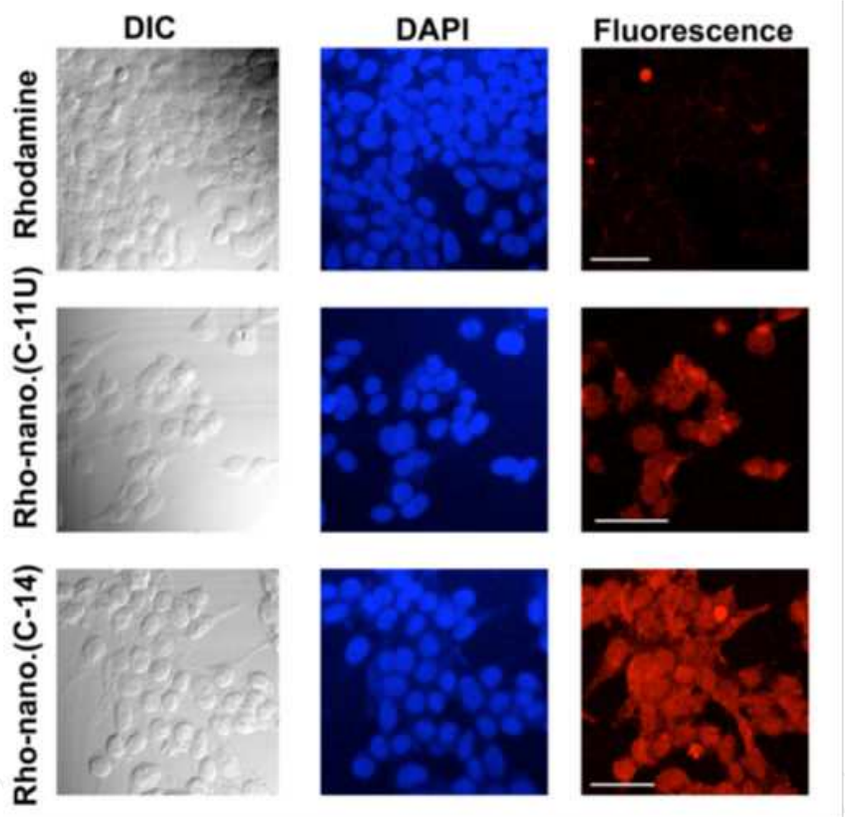

Figure 5. Uptake of raw rhodamine were compared to rhodamine containing nanoparticles uptake in HEK-293 cultured cell lines. Three separate sets of HEK-293 cells were cultures with raw rhodamine, C-11U and C-14 at 60 µg/ml concentration. The cells were fixed, processesd and viewed in a confocal microscope. Scale 50 µm.

The fruit fly, Drosophila melanogaster, is a good model for study cell biology with emphasis on toxicology (Peterson RT, Nass R, Boyd WA, Freedman JH, Dong K, Narahashi T. Use of non-mammalian alternative models for neurotoxicological study. Neurotoxicology. 29,546–555,2008). Here, we employed the Drosophila model to investigate nanoparticle interactions at different hierarchical scales of organization on Drosophilla at the egg, larval, and adult stages. PABA nanotubes and nanomaterials were mixed with yeast the standard Drosophila food at different concentrations, The food was seeded with 50 eggs of Drosophila melanogast-

er. After egg hatching (24 h), the larvae were observed to crawl through the food and ingest the suspended nanomaterials. Two of the fluorescent nanotubes were chosen for oral delivery. An important aspect of toxicity and genotoxicity studies is the selection of the assay system. Though In vitro approaches are preferred, the in vivo eukaryotic model, Drosophila appears as an ideal model organism. This has been already used to evaluate the internalization of nanoparticles and to solve open questions concerning cell uptake and live tissue distribution [27, 30]. The organic nanotubes when delivered through the food to the larval stage had no detectable effect on egg to adult survivorship.

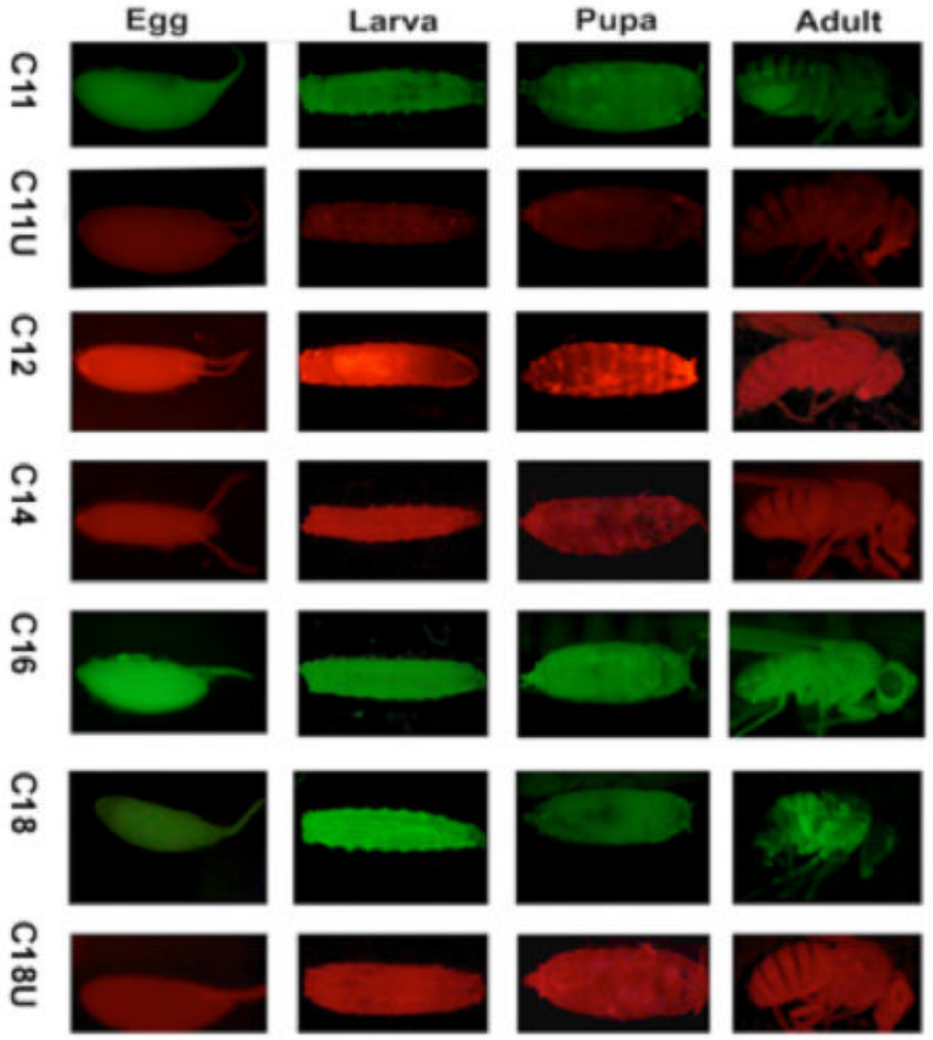

Figure 6. Biocompatibility and distribution of nanoparticles in four different developmental stages of Drosophila progeny after feeding nanomaterials containing media of the parental population.

Effect of nanoparticles on cell viability and cytotoxicity To address cell viability and cytotoxicity, colorimetric assay was performed using 3-(4-5-dimethylthiazol-2-yl)-2,5-diphenyltetrazoliumbromide. The cells incubated in freshly prepared nanoparticles containing media were treated with MTT. Uptake of nanoparticles in all cell types does not disturb normal cell

http://dx.doi.org/10.5772/58412

propagation and showed more than 90% cell viability even at the higher nanomaterial concentration (120 μg/ml) relative to DMSO treated cells. These results suggest that nanomaterials function as efficient bio-transporters and fail to show any cytotoxicity. These findings were further verified by a parallel study using flow-cytometry measurements. The mitotic cells from confluent cultures incubated with different nanomaterials containing media were assayed. The relative progression of cells from G1 to S phase was also determined. In three separate cultures containing 0 μg/ ml, 30 μg/ml, 60 μg/ml nanoparticles, the phases of cell cycles were progressing normally based on the incubation time, but in higher concentration (120 μg/ml), a fall of G1 number with concurrent increase in G2 and S phase was noticed indicating progression towards asynchrony.

To obtain visual images of assemblies including 3D structure and measurements, many images from fluorescent laser confocal microscope, scanning electron microscope (SEM) were analyzed. The 3D images showed that self-assembled structures, Benzamide microtubes (BAMT-A and BAMT-B) form tube like structure with a hollow space inside. Tubes are nearly 0.178 to 0.207 μm in width. The BAMT-A shows green fluorescence colour that emits from self-assembled 4-alkylamido-N-pyridin-2yl-benzamides coupling with a stearic side chain (C=18). Compound BAMT-B conjugated with a shorter lauric side chain (C=12) does not emit intrinsic fluorescence colour. To add standard fluorescence dye (Rhodamine B, red), BAMT-B organic tubular structure was manufactured by mixing Rhodamine B with tube-forming benzamide during the self-assembly process. The Rhodamine B that is embedded in the surface wall of self-assembled microtubes (BAMT-B) emits red fluorescence as specific signal. Both microstructures with variable side chains are DMSO and ethyl alcohol soluble, but not in water and can be stored for prolonged periods without loosing its organic properties.

Next insect and mammalian cells were used to estimate the efficiency of cellular uptake of two microtubes in vitro. Drosophila S2 cells, nonneoplastic Human Embryonic Kidney (HEK-293) (Figure 2A, B) and neoplastic HeLa cells were grown in small dishes or cover glasses and incubated with the microstructures dissolved in 0.1% DMSO that has no adverse effect on cell physiology (14). After 24 or 48 hrs incubations, cells were fixed in 4% paraformaldehyde, followed by few gentle washes with PBS. The cells were viewed under laser confocal microscope (Olympus FV1000). The reconstituted images showed that both BAMT-A and BAMT-B was accumulated in the periphery of the nucleus of both insect and human cells incubated with 60mg/ml microtubes containing 0.1% DMSO (Figure 2 a,b). The accumulation is increased proportionately to the concentration of microtubes ingested. In contrast, a negligible amount of fluorescence signals was emitted from the cells incubated in 0.1% DMSO alone for the same period of time. These findings demonstrated that microstructures are accumulated in the cultured cell after penetrating the plasma membrane. Moreover, an identical distribution pattern of BAMT-A and BAMT-B in the insect and human cells further verify that similar to intrinsic green in BAMT-A, embedded red fluorophore remains coupled with BAMT-B tube wall after accumulation in the cytosol.

Next to test the viability of the culture cells, a colorimetric assay was performed using 3-(4-5-dimethylthiazol-2-yl)-2,5-diphenyltetrazolium bromide as described earlier. This assay is based on the reductive capacity to metabolize the tetrazolium salt to blue coloured formazone.

Cells were incubated with various concentrations of microtubes. After incubation, cells were added with MTT and the absorbance of coloured product was monitored in a microplate reader at 570nm. In all the cases tested, the cell proliferation estimated by the absorbance and the viability of tumor HeLa and non cancerous HEK-293 cells in the presence of microtubes showed more than 95% viability relative to DMSO treated cells (Figure 2C). These results suggest that microstructures are the efficient molecular transporters for different biologically important cells with no cytotoxicity.

Further, these microsized structures were scaled up for *in vivo* use precisely to facilitate organ distribution and to combat different physiological hurdles in live organisms. To test overall viability and growth, after feeding the PABA containing microtubes to larvae, pupae and adult Drosophila were estimated. After hatching, larvae undergo an intense 4-5 day feeding, when they increase weight by 200-folds. In subsequent immobile pupal stage, they stop feeding, therefore no marked gain in adult fly weight from the larval stage is noticed. To feed larvae with highest possible doses of BAMT-A and BAMT-B, dry Baker's yeast was mixed with concentrated suspensions of microstructures (60μg in 100μl) in 0.1 % DMSO solutions, followed by centrifugation and decantation. The resulting pastes were used in equal amount as the sole food source for various batches of equal number of larvae. Indeed viability of the larvae, pupae and adult was marginally higher in sole DMSO (0.1%) fed flies relative to the flies fed on yeast paste containing microtubes (Figure 3). The feeding of low percentage DMSO (0.1%) has no apparent effect on fly physiology and viability. To investigate the effect of the microtubes on overall growth, behaviour and physiology of the flies, the size of the adults and the sexual behaviour of newly emerged flies were estimated. No size difference between DMSO and BAMT-A and BAMT-B fed male and female flies and abnormalities in their sexual behaviour were marked (Figure 3). The egg laying capacity of adult females for six consecutive days after hatching and the sex of eclosed flies were counted. No significant difference was detected in egg laying capacity and male/female ratios when compared to the wild type, DMSO or microtubes fed females (Figure 3). Taken together organic microtubes and their side alkyl chain modifications have no adverse effect on cellular physiology, behaviour, and sensitivity of fly sex and other pharmacokinetics parameters of live cells in the insects.(same as publication)

Organic nanotubes claimed a greater stability and better self-life and biocompatibility. To verify such claim of orally ingested microtube in live organisms, we reared the newly hatched adult flies, generated from microtubes or DMSO fed larvae, in the normal culture media for 7 consecutive days and examined under fluorescence microscope. Nearly equal level of fluorescence intensity was found from body parts of the adult flies reared in normal food media for 0 to 7 days (Figure 3d). Culture in food media without microtubes does not reduce the stability and self-life of the fluorescence organic microtubes for a limited period. The fluorescence intensity was reduced conspicuously after extending the culture on an average of 23-25 days and was eliminated within 47 days from the organs of the adult flies reared in the normal media. We further examined fluorescence intensity of the mature fertilized eggs laid by adult females reared in normal food for 7 days after hatching. No fluorescence signal was emitted from the eggs (Figure 3d). It eliminates the rare possibility of genetic inheritance of micro-

structures in the next successive generations through germ cells. Therefore, lack of heritable transfer of microtubes leads to an ineffective route of microtube spreading in the environment and their natural entry into the foodchain via participating consumers.

In live insects, majority of the internal organs are submerged in haemolymph – a blood equivalent of human. The haemolymph circulate through the open vessel and pump the fluid in a fixed direction at the posterior body cavity by using a series of valves that prevent opposite haemolymph flow. As reported earlier by feeding single walled carbon nanotubes in intact fly postulated that the fluorescent methods are ideal for delivery and diagnostic application. Feeding of microtubes in larvae and adults causes systemic spreading of signals by the gut peristaltic movement to cross the cell membrane barrier. The intensity of the dye associated with the microsized materials is proportionate to the amount of accumulated tubes that were incorporated in the gut cells. Variable intensity of fluorescent dyes in different parts of the body demonstrates different amounts of microtube accumulation in the different organs. Internal organs of larvae and adult tissues were dissected, fixed in 4% paraformaldehyde, processed and scanned under Confocal Fluorescence Microscope. At least five samples of each organ from larvae fed on microtubes were viewed and intensity of fluorescence scored (Supplementary Material). The amount of fluorescence of each tissue of the DMSO and microtube fed larvae and adults was estimated (Gray value/pixel) using Metamorph software. An increased accumulation of fluorescence dye was found in the digestive track (83.06+4.51 in BAMT-A), Malpighian tubules (57.19+3.81), fat bodies (38.41+2.19) compared to the salivary glands (27.73+1.81) and rapidly dividing cells of two imaginal discs (11.52+0.56 in wing discs and 14.32+0.41 in eye discs) (Figure 4). However, variable lengths of the side chains lead to the conspicuous changes in microtubes distribution at the different body parts. Shorter length of lauric side chain exhibited greater accumulation of microstructure. The cells of different discs and larval brain were devoid of any BAMT-A tubes containing longer side chain (C=18) but a considerable amount of BAMT-B (C=12) penetrated the same tissues after feeding equal amount of microtubes (Figure 4). In adults, a distinct pattern of BAMT-A and BAMT-B distribution in different organs was found. BAMT-A mainly accumulated in the abdomen, thorax including haltere and leg assuming their prolonged retention in the body fluid, while BAMT-B conjugated with C-12 side chain widely distributed in eye, antennae, proboscis and adult brain (Figure 4). To examine the preferential penetration of two side chains in adult brains, the amount of dyes in the brain tissue were tested. The BAMT-B with short side chain has a clear advantage in the entry of the brain tissue over BAMT-A in equal concentration. Interestingly, no change in fly behaviour after oral digestion suggest that accumulation of PABA microstructure do not produce any permanent damage in the brain because p-amino-benzoic acid functions in the improvement of neuro-degerative damages by inhibiting acetylcholinesterase.

Further high concentrations of fluorescence conjugated with BAMR-B were observed in insect cells and in all the organs of Drosophila after feeding. Enlarged view of insect cells and wing disc (Figure 4) verified the accumulation of micro-structure in the cytoplasm of cultured cells and fixed tissues. These finding allowed us to confirm the physical accumulation of microtubes in both cell types. In contrast, low abundance of the BAMT-A

microtubes in the salivary glands and rapidly dividing cells of imaginal discs probably represent the secondary uptake after the microtubes enter into the haemolymph. These findings demonstrate that differential uptake and specificity of live cell targeting by the microtubes depend on the cellular physiology, chemical modification of carrier to travel and enter live cells.

Here, several critical questions relevant to biocompatibility and application of p-aminozbenzoic containing microstructures are addressed. (1) It determines the parameters of chemical and biological modifications suitable for oral administration. However, the impact on specific cellular physiology and efficient uptake of microstructures by carrier molecules based on their chemical modifications cannot be ignored. It is evident that distribution and accumulation is prone to shorter (C=12) alkyl side chain. (2) These organic microtubes overcome cell physiological, pharmacokinetic barriers and show an efficient cellular uptake in animal cultured cells (5,19). (3) It has no adverse effects in physiology, behaviour and growth of insects that shows strong similaries with human at molecular level (3) Finally, modifications in alkyl side chain play an important role in biodistribution. The side chain modifications in BAMT-A and BAMT-B alter the shape of microstructures by changing self assembly properties and discriminate tissue specific distribution specifically in adult eye, its precursor cells, wing imaginal discs and neuronal tissues in larval and adult brain but do not show any conspicuous changes of their biodistribution in cultured insect and human cells. The chemical modifications of self assembled p-aminobenzoic moiety also show a better stability and long self-life before degradation but no short-term toxicity, impaired growth of Drosophila larvae and adults after feeding solely on microtubes containing media. Moreover, no obvious effect on fecundity or impairment of fertility was noticed in the adult female flies. During self assembly, chemical modifications of PABA, and their longer stability in the internal organs provides the microtubes as better-suited and sustainable cargo in live organisms, unlike inorganic nanomaterials that neither accumulate in the live cells nor produce cytotoxicity in the cellular environment. Most logical extension of this work would be the cell specific target delivery in which coupled small molecule on the surface wall have define properties for attachment of specific cell surface and/or stringent proteins for facilitating antigen-antibody reactions. This approach could be used not only to deliver small regulatory RNA and DNA as therapeutic materials but also to optimize pill like properties for oral ingestion with no pharmacokinetic barriers. Though this study used only one structure moiety of drug molecules, it is likely that the method would work with other types organic microstructure as long as three major criteria of orally administered molecule biocompatibility, pharmacokinetics and a capacity for multivalency are considered. Therefore chemical modulations on the surface should be incorporated in the design to attach the multivalency of small ligands. These changes in organic microstructure were described recently. Such attempts for synthesizing tissue or cell guided orally ingested microstructure may favour to make the next generation micropill to deliver biomaterials for effective gene therapy and novel cargo useful for molecular diagnostics.

http://dx.doi.org/10.5772/58412

6. Mode of uptake of PABA nanomaterials

Broadly, there are two modes of entries, either PABA nano-materials transverse the cell membrane via endocytosis orenergy independent nonendocytotic mechanism. We have carried out a series of investigations on uptake mechanism and cellular internalization for PABA conjugates. Endocytosis is an energy dependent mechanism. The process is hindered at a low temperature (at 4°C instead of 37°C) or in ATP deficient environment. Cells incubated in media containing nanoparticles were either cultured at 4°C or pretreated with NaN3 for inhibiting the production of ATP, thereby hampering the endocytosis process. The level of fluorescent intensity in the cytosol of each cultured cells was reduced dramatically relative to cells cultured in regular standard conditions (Figure 3). This reduction determines that PABA conjugates enter in the sub-cellular compartment of cultured cells via endocytosis. We also sub-categorized the endocytosis pathway including phagocytosis, pinocytosis, clathrin dependent receptor mediated and clathrin independent mechanisms.Internalization often occurs when the clathrin coat on the plasma membrane forms conspicuous invagination in the cell membrane leading to the budding of clathrin-coated vesicles. As a result, extracellular species located on the cell membrane are trapped within the vesicles and invaginated inside the cells. To disrupt the formation of clathrin coated vesicles on the cell membranes, cells were preincubated in sucrose (hypertonic) soluton or K+-depleted media before treatment with all seven nano-particles. Data showed a drastic reduction in PABA nano-particle uptake (Figure 3C), which suggests that a clathrin dependent endocytosis process is involved in entry mechanism.

7. Uptake of PABA nanomaterials by clathrin dependent endocytosis

To rule out the possibility of cellular uptake of PABA conjugates via caveolae or lipid rafts pathway, we pre-treated the cells with drug filipin and nystatin, which disrupt cholesterol distribution within the cell membrane. In contrast to clathrin blocking experiments, pre-treatment of the drugs had a negligible blockage on the cellular uptake, which suggests a little or no involvement of the caveolae dependent cell entry. In a similar control experiment we studied the uptake of fluroscent labelled cholera toxin B (CTX-B) which is a multivalent ligand protein known to be internalised by caveolae depenent endocytic pathway (Figure 3E). The CTX-B showed a significant inhibition in cell entry in the presence of filipin and nystatin. Taken together, the results verify that cellular internalization of PABA conjugates is mediated through the clathrin-dependent endocytosis pathway.

8. Oral uptake of variable PABA nanomaterials in Drosophila

Organic nano-assemblies have negligible adverse effect on cellular physiology, behaviour, sensitivity to adult sex and other pharmacokinetics parameters of Drosophila. We have screened nanoparticles conjugated with variable side chains for organ specific targeting in

Drosophila. Different sets of larvae, pupae and adult flies were grown with sole feeding of nanoparticle containing media. The accumulation to various tissues, selective organ uptake and their clearance was also monitored by imaging the fluorescence signals during the stages of development in Drosophila. In live insects, oral feeding of nanomaterials causes systemic spreading of signals through the gut by peristaltic movement tocross the cell membrane barrier. In general, majority of the nanoparticles carrying unsaturated side chains (C-11U, C-18U) showed a low level of incorporation in all stages of Drosophila life cycle although C-18U showed a comparatively high level of incorporation in two different life stages, larvae and pupae (Additional File 2 Figure S16A-B). We further investigated the efficacy of in vivo targeted delivery among nanoparticles that emits intrinsic green and nanoparticles with intercalated rhodamine B in the wall. Intrinsic green nanostructures carrying C-16 side chain showed a maximum amount of incorporation through cell membranes, compared to C-18, and C-11 that showed a variable amount of incorporation in different developmental stages. Animals fed with C-18 selfassembled particles exhibit a maximum incorporation during larval stage as compared to other tested stages. Animals fed with C11 showed an overall low level of entry in all the stages of development.

Delivery of rhodamine B embedded nanoparticlesC-12 showed an equal and maximal level of incorporation in all stages of development. The intensity was conspicuously greater than the nano-structure carrying C-14 chain. Taken together, specific carbon chains and associated morphologies of nanostructures brought a potential difference in entry through gut cell walls. These results suggest the possibility that the physiology of gut cells in different stages of the life cycle might influence nanoparticles uptake.

For in vivo tracking, fluorescence dyes attached to nanoparticles suffer with multiple problems including photo-bleaching and ability to interrogate multiple targets etc. The aftermath effect of such limitations of fluorescence imaging in live objects was described earlier. In all cases, during in vivo delivery there was no photobleaching of the nanomaterials through all stages of development providing a better advantage in tracking in live systems. But the fluorescence intensity was reduced conspicuously after extending the culture on an average of 18-25 days and nearly eliminated within 40-45 days allowing a total clearance of fluores-cence from the live tissues. We further screened the efficacy of nano-particles inheritance through germ cells. The adult flies emerging from sole feeding of nanoparticle containing media were cultured in normal food media for another 7 days. The fertilized eggs from different batches of flies after nanoparticle feeding emits only trace amount of fluorescent as a background effect. Therefore, this ineffective route of gem cell based heritable transmission prevents nanomaterials contamination in the environment and their natural entry into the food chain via eco-consumers.

9. Efficiency of organ specific delivery of PABA nanomaterials by side chain variation in Drosophila

To categorize the intensity of fluorescent molecules as an absolute reflection on efficacy of nanoparticle delivery, different internal body parts of the larvae were dissected and visualized

http://dx.doi.org/10.5772/58412

under fluorescence microscope. A wide range of variation in fluorescence intensity was observed in different larval body parts, for example mouth, brain, larval neural ganglia, salivary glands, alimentary canal and malpighian tubules etc (Figure 4; Additional File 2 Figure S16). A clear contrast was observed in the delivery of nanomaterials in the salivary glands. C-14 and C-18 containing nanostructures incorporated at a massive level in the glands but shows an intermediate level of incorporation in both neural tissues and organism itself (Figure 4). Surprisingly, we observed that malphigian tubules absorbed more nano-particles that emit intrinsic fluorescence. Therefore nanoparticles with different side chains showed a distinct distribution in various internal tissues in the larvae. Nanoparticle entry showed a clear variation in rapidly dividing cells of mature larval imaginal discs (the precursor organs of adult wings, eyes and legs). PABA conjugated with C-16 side chain showed a higher intensity of uptake in all three discs tested. However the intensity of fluorescence is moderate in C-11U, C-12 and C-18 particles (Figure 4). It suggests that the structure and surface texture of C-16 side chain is the most effective cargo for delivery in precursor and rapid dividing cells, though we cannot rule out other unmet criteria in the tracking process (Figure 4). As described above, the delivery of C-12 structure in all the stages of development is ideal compared to C-14 and nanomaterials with unsaturated side chains in C-11U and C-18U. Surprisingly a differential uptake of nanomaterials produced by C18 and C18U specially in leg discs that possess same number of carbon bonds interprets that length of the side chain is not an only criteria for nano-particles based delivery in imaginal discs.

The conjugated side chains of PABA nanostructures were also screened for delivery to complex adult body parts derived from same sets of larval imaginal discs. Entry of nanomaterials was analysed in adult eyes, halters and legs. Incorporation in adult eyes is complicated and novel from other body parts. Two different fluorescent tags showed distinct uptake through eye ommatidia (Figure 4) raising the possibility that difference in fluorophore emission and structure make their entry visible and distinct in adult eyes. The intrinsic green showed a poor emission through ommatidia. Only a trace amount of green colour was visualized whereas rhodamine B showed a greater intensity with a maximum incorporation of C-16 in the eyes. However, the incorporation pattern of nanomaterials conjugated with variable side chains in halters and legs is distinct from their distribution in eyes. Among all possible nanostructure, C-11U and C-18U were targeted orally at a maximal level to the legs while C-11, C-12 and C-16 in the halters showed an equal but greater amount of incorporation, which suggests that the unsaturated carbon chains have advantage for selective entry in the accessory organs of Drosophila. Taken together, the delivery of nanoparticles associated with variable side chains in the culture cells and in vivo uptake by oral delivery in different body parts is different.

Furthermore distribution of numerous neurons and other cells make brain more compact and the delivery of therapeutic agents in the neuronal tissues is the most challenging task. In spite of complicated entry in brain, two nanoparticles, C-11 and C-16 containing particles show a considerable amount of entry when incorporation of other particles is nominal in the brain (Figure 4). Truly, greater dissemination of nanostructures in adults, larvae and different body

parts including brains suggests that physio-chemical properties including shapes, surface texture of the C-11 and C-16 particles are the best-fitted materials (Figure 4).

10. Perspective

The key parameters of nanomaterials for easy and efficient delivery are shape, size and flexibility to enter and exit cell barrier. Our results clearly demonstrate that the properties of each acid side chain together with common PABA moiety influences size, shape and surface texture of nanomaterials that lead to differential uptakeand specificity in live cell delivery. The physio-chemical modifications of organic nano carriers also affect cell internalization mechanisms in sub-cellular organelles as found by distinct accumulation pattern of each nanomaterials following same energy dependent endocytosis. In vivo screening also showed that only C 11 and C-16 produce compatible shape and size of nanomaterials that are best fitted for easy delivery of PABA nanomterials. These results suggest that physical structure of nanomaterials and chemical properties of acid side chain required for self assemble procedure and size variation could be the initial step for cellular uptake.

In addition to cultured cells, tissue specific distribution specifically in adult eyes, imaginal discs, alimentary tracks and neuronal tissues was complex and needs more parameter to consider. Our data revealed that a complex interrelationship of PABA conjugates and cell physiological environment is important in live materials delivery. The internal tissue environment might provide additional barriers for nanomaterial entry as depicted by comparing variable accumulation of same nanomaterials in cross species; Drosophila and human cell lines. A similar difference was also noticed when C-11 or C16 accumulation was compared in multiple complex organ of Drosophila. However, nanomaterials compatible for oral delivery do not show any short-term toxicity, impaired growth of Drosophila larvae and adults. We hypothesize that two distinct parameter nano-skeleton frame with conjugated acid chains and live cell physiology are best suited for cell uptake and delivery to internal organs after oral consumption. Our results also differ from the hypothesis that nano-particle uptake in live cells occurred through energy independent non-endocytotic pathway involving insertions and diffusion across the cell membrane. Sub cellular internalization of PABA nanomaterials predominantly takes place by energy dependent endocytosis. Earlier we have found that PABA nanomaterials can penetrate plasma membrane in the human cells and enter into cytoplasm. The variable amount of different nanomaterial accumulation by energy dependent endo-cytosis in same cell type ruled out the possibility that a single internalization mechanism, endocytosis is exclusively required for uptake. However, a marked reduction of different nanomaterials under endocytosis inhibitory conditions believed that such discrepancies are due to sharp differences in size and shape of the self assembled structures. In addition as organic nanomaterials suffer from uncontrolled aggregation to form micron sized particles after prolong storage; thereby ruling out the possibility of insertion, diffusion and penetration mechanisms [22]. PABA nanoparticles have a high tendency to associate with cell membrane (Figure 2, 3).

Such accumulation might give rise to artefact in cellular uptake of micro-sized aggregates as found in artifactual intake of HIV TAT peptide at 4°C [23]. Therefore, cellular entry of PABA might depend on the size of the nanoparticles which is mainly guided by the acid side chain.

Finally, a systematic screening of PABA conjugated library provides sufficient evidences to support the following statements: 1) Two nanomaterials carrying C-11 and C16 acid side chains are best suited for optimal entry in cells and multiple organs. 2) In live tissues, an internal environment might be a useful barrier for improving nanoparticles delivery in multiple organs. 3) Cellular internalization or uptake mechanism of nanomaterials might unravel the clues for smooth entry in human cells and efficient delivery and 4) finally screening of PABA conjugates determine a functional relationship between energy dependent endocytosis and nanomaterial structure for each organ specific targeting.

11. Conclusions

We have shown that two carbon linker group C-11 and C-16 forms tubular nanomaterials that are best fitted for mass oral delivery in complex multiorgans. The cellular uptake mechanism is energy dependent endocytosis. The detailed endocytosis pathways for nano PABA structure is operated thorough clathrin-coated pits rather than caveolae or lipid rafts. In vivo screening of PABA nanomaterials produced by different acid side chain select the compatible nano structure ideal for oral delivery and establishes energy dependent entry mechanism is of fundamental importance that will facilitate future developments of PABA nanoparticle transporters for biological delivery application

Author details

Utpal Bhadra[1], Manika Pal Bhadra[2], Jagannadh Bulusu[3] and J.S. Yadav[4]

1 Functional Genomics & Gene Silencing Group, CSIR-Centre for Cellular & Molecular Biology, Hyderabad, India

2 Centre for Chemical Biology, CSIR-Indian Institute of Chemical Technology, Hyderabad, India

3 Division of Organic Chemistry-I, Indian Institute of Chemical Technology, Hyderabad, India

4 Ex-Director & CSIR Bhatnagar Fellow, Indian Institute of Chemical Technology, Hyderabad, India

We are highly sympathetic due to sudden demise of Dr Jagannath Bulusu and we hope his soul lies in peace

References

[1] Nichols HL, Zhang N, Zhang J, Shi D, Bhaduri S, Wen X. Coating nanothickness degradable films on nanocrystalline hydroxyapatite particles to improve the bonding strength between nanohydroxyapatite and degradable polymer matrix. J Biomed Mater Res A. 2007 82(2): 373-82.

[2] Dey D Goswami T. Optical biosensors: a revolution towards quantum nanoscale electronics device fabrication. J. Biomed. Biotechnol. 2011; 2011: 348218.

[3] Vikesland PJ, Wigginton KR. Nanomaterial enabled biosensors for pathogen monitoring-a review. Environ Sci Technol. 2010; 44(10): 3656-69.

[4] Zhang K, Zhang S, Luo Z, Wang J, Wang T, Ou G, Wang H. Biocompatibility of porous calcium phosphate ceramic nanocomposite. Hua Xi Kou Qiang Yi Xue Za Zhi. 2012; 30(2): 209-13.

[5] van Hameren R, Schön P, van Buul AM, Hoogboom J, Lazarenko SV, Gerritsen JW, Engelkamp H, Christianen PC, Heus HA, Maan JC, Rasing T, Speller S, Rowan AE, Elemans JA, Nolte RJ. Macroscopic hierarchical surface patterning of porphyrin trimers via self-assembly and dewetting. Science 2006; 314(5804): 1433-6.

[6] J.S. Yadav and Manoj K. Gupta. Self-assembled lipid nanotubes, nanosheets and nanopipes. IJPSR, 2012; Vol. 3(12): 4822-4826

[7] Salvador-Morales C, Valencia PM, Thakkar AB, Swanson EW, Langer R. Recent developments in multifunctional hybrid nanoparticles: opportunities and challenges in cancer therapy. Front Biosci (Elite Ed). 2012; 4: 529-45.

[8] Wang Y, Chen L. Quantum dots, lighting up the research and development of nanomedicine. Nanomedicine. 2011; 7(4): 385-402

[9] Kairdolf BA, Smith AM, Stokes TH, Wang MD, Young AN, Nie S. Semiconductor quantum dots for bioimaging and biodiagnostic applications. Annu Rev Anal Chem (Palo Alto Calif). 2013; 6: 143-62.

[10] Guo Y, Shi D, Lian J, Dong Z, Wang W, Cho H, Liu G, Wang L, Ewing RC. Quantum dot conjugated hydroxylapatite nanoparticles for in vivo imaging. Nanotechnology. 2008; 19(17): 175102.

[11] Maiorano G, Rizzello L, Malvindi MA, Shankar SS, Martiradonna L, Falqui A, Cingolani R, Pompa PP. Monodispersed and size-controlled multibranched gold nanoparticles with nanoscale tuning of surface morphology. Nanoscale. 2011; 3(5): 2227-32.

[12] Tang L, Cheng J. Nonporous Silica Nanoparticles for Nanomedicine Application. Nano Today. 2013; 8(3): 290-312.

[13] Naskar J, Banerjee A. Concentration dependent transformation of oligopeptide based nanovesicles to nanotubes and an application of nanovesicles. Chem Asian J. 2009; 4(12): 1817-23.

[14] Kim W, Thévenot J, Ibarboure E, Lecommandoux S, Chaikof EL. Self-assembly of thermally responsive amphiphilic diblock copolypeptides into spherical micellar nanoparticles. Angew Chem Int Ed Engl. 2010; 49(25): 4257-60.

[15] Perez JM, O'Loughin T, Simeone FJ, Weissleder R, Josephson L. DNA-based magnetic nanoparticle assembly acts as a magnetic relaxation nanoswitch allowing screening of DNA-cleaving agents. J Am Chem Soc. 2002; 124(12): 2856-7.

[16] Ennio Tasciotti, Xuewu Liu, Rohan Bhavane, Kevin Plant, Ashley D. Leonard, B. Katherine Price, Mark Ming-Cheng Cheng, Paolo Decuzzi, James M. Tour, Fredika Robertson & Mauro Ferrar. Mesoporous silicon particles as a multistage delivery system for imaging and therapeutic applications. Nature Nanotechnology 2008; 3, 151 – 157.

[17] Albanese A, Tang PS, Chan WC. The effect of nanoparticle size, shape, and surface chemistry on biological systems. Annu Rev Biomed Eng. 2012; 14: 1-16.

[18] Sahay G, Alakhova DY, Kabanov AV. Endocytosis of nanomedicines. J Control Release. 2010; 145(3): 182-95

[19] Akerman ME, Chan WC, Laakkonen P, Bhatia SN, Ruoslahti E. Nanocrystal targeting in vivo. Proc Natl Acad Sci U S A. 2002; 99(20): 12617-21.

[20] Weissleder R, Kelly K, Sun EY, Shtatland T, Josephson L: Cell-specific targeting of nanoparticles by multivalent attachment of small molecules. Nat Biotechnol 2005, 23:1418-1423

[21] Kluczyk A, Popek T, Kiyota T, de Macedo P, Stefanowicz P, Lazar C, Konishi Y. Drug evolution: p-aminobenzoic acid as a building block. Curr Med Chem. 2002; 9(21): 1871-92.

[22] Schmelke, F. C. & Rubin, M. *J. Am. Chem. Soc.* 1944; 66, 1631.

[23] Chen Y, Zhu B, Zhang F, Han Y, Bo Z. Hierarchical supramolecular self-assembly of nanotubes and layered sheets. Angew Chem Int Ed Engl. 2008; 47(32): 6015-8.

[24] Han M, Hyun J, Sim E. Formation of rigid organic nanotubes with controlled internal cavity based on frustrated aggregate internal rearrangement mechanism. J Phys Chem B. 2013; 117(25): 7763-70.

[25] Wilner OI, Orbach R, Henning A, Teller C, Yehezkeli O, Mertig M, Harries D, Willner I. Self-assembly of DNA nanotubes with controllable diameters. Nat Commun. 2011; 2:540.

[26] Wu Y, Xiang J, Yang C, Lu W, Lieber CM. Single-crystal metallic nanowires and metal/semiconductor nanowire heterostructures. Nature. 2004; 430(6995): 61-5.

[27] Yadav JS, Lavanya MP, Das PP, Bag I, Krishnan A, Jagannadh B, Mohapatra DK, Bhadra MP, Bhadra U: 4-N-pyridin-2-yl-benzamide nanotubes compatible with mouse stem cell and oral delivery in Drosophila. Nanotechnology 2010; 21: 209802.

[28] Stuart L. Schreiber. Target-Oriented and Diversity-Oriented Organic Synthesis in Drug Discovery. Science 2000; 287(5460): 1964-1969

[29] Peer D, Park EJ, Morishita Y, Carman CV, Shimaoka M. Systemic leukocyte-directed siRNA delivery revealing cyclin D1 as an anti-inflammatory target. Science. 2008; 319(5863): 627-30.

[30] Yadav JS, Das PP, Reddy TL, Bag I, Lavanya PM, Jagannadh B, Mohapatra DK, Bhadra MP, Bhadra U: Sub-cellular internalization and organ specific oral delivery of PABA nanoparticles by side chain variation. J. Nanobiotechnology, 2011, 9, 10.